Alpha-cluster spectroscopy in ^{40}Ca and in the *sd*-shell closure region

G. Reidemeister
Physique Nucléaire Théorique et Physique Mathématique, Université Libre de Bruxelles, B-1050 Bruxelles, Belgium

S. Ohkubo
Department of Applied Science, Kochi Women's University, Kochi 780, Japan

F. Michel
Faculté des Sciences, Université de l'Etat, B-7000 Mons, Belgium
(Received 25 September 1989)

The low-energy ^{36}Ar(α,α) elastic scattering data of Gaul *et al.* are analyzed within the frame of the optical model, using energy-independent Woods-Saxon squared or model-independent geometries for the real part of the potential. The optical-model scattering amplitude is decomposed into its barrier and internal wave components to understand the rapid and complicated evolution of the angular distributions with incident energy. The properties of the low-energy bound and quasi-bound states supported by this potential are compared with those of the states of the deformed 4p-4h rotational band in ^{40}Ca, built on the $J^\pi=0^+$, $E_x=3.35$ MeV state. The possibility of extending this local potential model approach to neighboring nuclei near the *sd*-shell closure is discussed. A negative-parity band of states with appreciable α-cluster character, starting around the α-particle threshold, is expected to be systematically present in this mass region.

I. INTRODUCTION

There is now convincing evidence that the α-cluster description of low-lying nuclear levels—which has proved so successful for understanding the properties of light nuclei of the *sd*-shell region[1]—can be extended to the beginning of the *fp* shell. Local potential model (LPM) calculations of the α-cluster structure of ^{44}Ti,[2] starting from the unique optical potential describing elastic ^{40}Ca(α,α) scattering on broad angular and energy ranges,[3] predict the existence of various α-cluster states, which group into quasirotational bands, with properties not dissimilar to those displayed by the well-understood ^{20}Ne nucleus, of which ^{44}Ti is the *fp*-shell analog. These findings have recently been substantiated by semimicroscopic[4] and microscopic[5] calculations, which confirm that insisting upon the continuity of the cluster description from negative energy properties to the scattering regime[2] eliminates most of the uncertainties related to the choice of the effective interaction used in the calculations.

Both the LPM and these microscopic calculations produce as the lowest band a positive-parity band of states with moderate cluster character at low spin, with properties agreeing well with those of the experimental ^{44}Ti ground state band. They predict in addition an excited positive-parity band with strong cluster character, starting a few MeV above the $\alpha+^{40}$Ca threshold. The states of this band with spins ranging from 6 to 12 have recently been shown[6] to be responsible for the broad oscillations seen in the experimental $\alpha+^{40}$Ca fusion excitation function; this band is the close analog of the famous "higher nodal" $K^\pi=0_4^+$ band in ^{20}Ne.[1] Midway between these two bands, a negative-parity band, starting just above the $\alpha+^{40}$Ca threshold, and composed of narrow states with intermediate cluster character, is invariably predicted;[2] although it has up to now no experimental counterpart, this band, which is the analog of the "inversion-doublet" $K^\pi=0^-$ band in ^{20}Ne,[1] should be actively searched for since its observation would definitely confirm the present picture. Further broad and overlapping cluster states are predicted at higher energies; these states play an important role in enhancing the ^{40}Ca(α,α) backward angle cross section.[2]

It is well known that the band structure of some of the excited states of the ^{16}O nucleus can be interpreted in a weak coupling picture where the ^{20}Ne ground state band is coupled to the ^{12}C ground state.[1] Indeed both the positive-parity band built on the $J^\pi=0^+$, $E_x=6.05$ MeV level, and its "inversion-doublet" negative-parity partner built on the $J^\pi=1^-$, $E_x=9.58$ MeV state, with strong cluster character, have been interpreted as composed of states having the structure of an α-particle orbiting a (deformed) unexcited ^{12}C core; higher-lying bands have likewise been interpreted as corresponding to the motion of the cluster around the ^{12}C core excited to its $J^\pi=2^+$, $E_x=4.43$ MeV first rotational level.

There exists in the ^{40}Ca nucleus a famous rotational band built on the deformed $J^\pi=0^+$, $E_x=3.35$ MeV excited state; this band has been shown by Gerace and Green[7] and by Federman and Pittel[8] to correspond to a 4p-4h excitation. This band has repeatedly been interpreted within a weak coupling picture where the ^{44}Ti ground state band is coupled to the ^{36}Ar ground state; Indeed, apart from a substantial difference in the 0^+-2^+ spacing, the two bands are remarkably similar up to a global shift in energy of some 1 MeV.[9]

One can inquire whether this weak coupling picture extends to higher-lying bands of the $\alpha+^{36}$Ar system. If this is the case, ^{36}Ar(α,α) elastic scattering should be describable in terms of an optical potential with a real part very similar to that used for ^{40}Ca(α,α) scattering, and the bound and quasibound states supported by this potential should group into bands similar to those disclosed by the $\alpha+^{40}$Ca calculations. In particular it is interesting to investigate the persistency of a possible negative-parity "inversion-doublet" band in this system, and to study what are the prospects of identifying it experimentally. More generally it is relevant to discuss the persistency of α-particle cluster structure in the region of the *sd*-shell closure; this possibility—which, it is worth recalling, had already been suggested some 30 years ago in a pioneering paper by Sheline and Wildermuth[10]—can now be reinvestigated with better prospects in view of the recent progress made in the field.

The organization of our paper is as follows. In Sec. II we present the results of an optical-model analysis of the few available ^{36}Ar(α,α) elastic scattering data, and we investigate the scattering properties of the extracted potentials; Sec. III is devoted to the study of the bound and quasibound state properties of the potentials in connection with the α-cluster spectroscopy of ^{40}Ca. Preliminary reports of these results have been presented in Refs. 11 and 12. Finally, we discuss and extend these results to several nearby systems in Sec. IV, and we present a summary and our conclusions in Sec. V.

II. OPTICAL-MODEL ANALYSIS OF THE $\alpha+^{36}$Ar ELASTIC SCATTERING DATA

In contrast with the case of the $\alpha+^{40}$Ca system, whose scattering properties were studied comprehensively by several experimental groups, the $\alpha+^{36}$Ar system has received comparatively little attention. Indeed to our knowledge the only available experimental data extending on the whole angular range are those of Gaul *et al.*,[13] obtained at the four incident energies $E_\alpha=18.0$, 22.1, 24.1, and 29.2 MeV, and older data of Boschitz *et al.*[14] at 31.8 and 41.0 MeV. There exist also lower-energy data covering the range $12.8\leq E_\alpha\leq 17.8$ MeV due to Wallace *et al.*,[15] but because of the interplay with compound elastic scattering at these energies they are less suited to the type of optical-model analysis we are considering here.

All these data display—although to a lesser extent—the same type of backward angle anomaly as that evidenced by the more popular $\alpha+^{40}$Ca system. In this latter case it is known that the "anomalous" large angle scattering (ALAS) observed at low energy can be described quantitatively within the frame of the optical model, provided use is made of a convenient real form factor and of an absorptive potential significantly weaker than for neighboring systems.[3,16] Although because of the familiar discrete ambiguity several potential "families" coexist at low energy, a single family is able to describe correctly the progressive disappearance of the backangle anomaly and the transition towards the higher-energy rainbow scattering regime. This potential is best characterized by its volume integral per nucleon pair, which assumes values varying between 350 and 370 MeV fm^3 at low incident energy; this volume integral decreases slowly with incident energy, with a slope of some 0.7 MeV fm^3 per MeV. It is also relevant to recall that because of the particularly low absorption the real part of this potential is determined with exceptional accuracy on a wide radial range, as has been shown by Gubler *et al.*[17] in their model-independent analysis of the data.

We have subjected the ^{36}Ar(α,α_0) data of Gaul *et al.*[13] to an optical-model analysis. As no data were available at sufficiently high energy to resolve the discrete ambiguity the analysis was restricted to the potential family with a volume integral per nucleon pair nearest to that obtained for the $\alpha+^{40}$Ca system.[3] Two searches were actually conducted independently. In one of these,[12] use was made of Woods-Saxon squared form factors for the real and imaginary parts of the potential $U(r)$:

$$U(r)=-V_0 f(r;R_r,a_r)-iW_0 f(r;R_i,a_i)\ , \tag{1}$$

with

$$f(r;R,a)=\{1+\exp[(r-R)/a]\}^{-2}\ . \tag{2}$$

It proved possible to obtain a satisfactory agreement with the data using an energy-independent real part and a fixed imaginary geometry; the resulting parameters are $V_0=185$ MeV, $R_r=4.590$ fm, $a_r=1.210$ fm, $R_i=4.623$ fm, $a_i=1.00$ fm, while W_0 took on the values $W_0=17$, 19, 21, and 23 MeV at $E_\alpha=18.0$, 22.1, 24.1, and 29.2 MeV incident energies, respectively. As can be seen from Fig. 1, the essential features of the data, which display very rapid changes with incident energy on the restricted range considered here, are remarkably described by the model.

An independent search[11] was conducted using a more flexible form factor for the real part of the potential, that is, a model-independent geometry of the spline type; the imaginary part was restricted to a Woods-Saxon squared geometry as above. The analysis was started using the 29.2 MeV $\alpha+^{36}$Ar potential of Ref. 16, where a model-independent analysis was carried out in order to investigate the energy and mass dependence of ALAS around $A=40$. In order to keep the number of variable parameters to a minimum, an energy-independent geometry was used for both the real and imaginary parts of the potential, and in view of the insensitivity of the calculated cross sections to the very inside part of the interaction the real geometry was regularized by assigning fixed potential depths at the first four points of the $\Delta r=1$ fm spline mesh.

An excellent agreement with the data could be achieved in this way, as can be judged from Fig. 1; the only energy-dependent parameters are the normalization factors λ and W_0 of the real and imaginary wells (by definition λ is taken equal to 1 at 24.1 MeV incident energy). It is worth stressing again how good the agreement with experiment is in view of the seemingly hectic energy behavior of the data analyzed here. It has also to be pointed out that the 18 MeV data are likely to include a non-negligible compound elastic contribution, as is re-

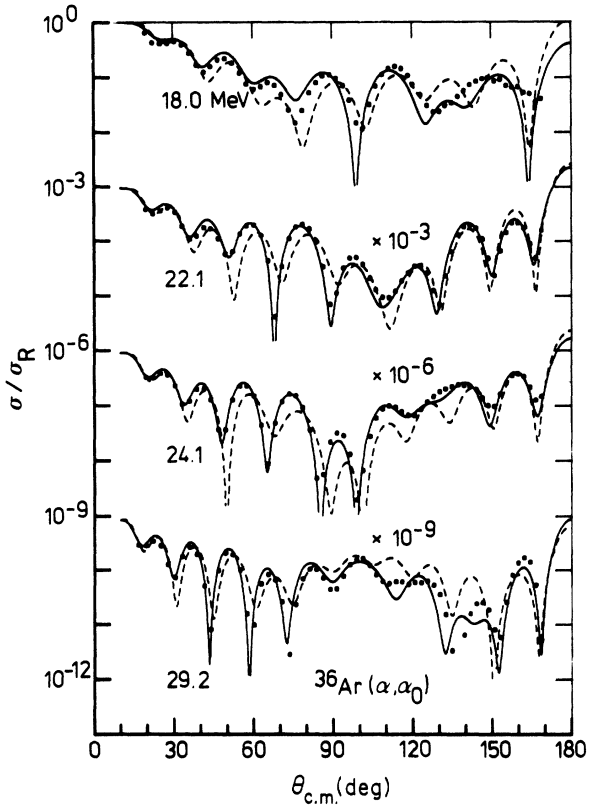

FIG. 1. Comparison of the predictions of the Woods-Saxon squared potential (dashed line) and the spline potential (solid line) with the experimental ^{36}Ar(α,α_0) data of Gaul *et al.*[13] (circles).

vealed by the analysis of Wallace *et al.*;[15] the compound elastic cross section is, however, decreasing rapidly with incident energy, so that from 22.1 MeV onward we expect this contribution to be of minor importance.

The real parts of the two potentials at $E_\alpha = 24.1$ MeV are compared in Fig. 2; except for departures of limited amplitude in the surface ($r \simeq 5$ fm) and in the far tail regions they are seen to be in essential agreement. Also shown for comparison is the real part of the 24 MeV $\alpha + ^{40}$Ca Woods-Saxon squared potential,[2] which, as expected, extends slightly farther out than its $\alpha + ^{36}$Ar counterparts. Attempts to avoid the "knee" in the $\alpha + ^{36}$Ar spline potential around 6 fm systematically resulted in inferior fits to the data, whatever the imaginary geometry used in the analysis. This feature could possibly reflect the effect of coupling to inelastic (rotational) excitations of the deformed ^{36}Ar target, which when treated implicitly by incorporating them in the optical potential are expected to contribute mainly in the surface region.[18]

The volume integral per nucleon pair of the real part of the energy-independent potential of Eqs. (1) and (2), which takes the value $J_v/4A = 374$ MeV fm^3, is comparable to that assumed by the real part of the spline potential; the latter is equal to 355.0, 352.8, 352.1, and 347.5 MeV fm^3 at 18.0, 22.1, 24.1, and 29.2 MeV incident energies, respectively. The imaginary volume integrals likewise take on similar values in the two descriptions; they amount to 34.9, 39.0, 43.1, and 47.2 MeV fm^3 for the

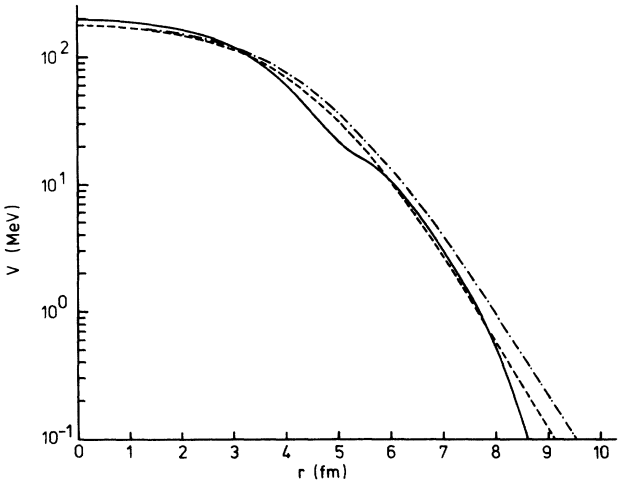

FIG. 2. Real parts of the $\alpha + ^{36}$Ar optical potentials extracted at $E_\alpha = 24.1$ MeV: Woods-Saxon squared potential (dashed line) and spline potential (solid line). The $\alpha + ^{40}$Ca potential[2] at the same incident energy is also shown for comparison (dot-dashed line).

Woods-Saxon squared potential, and to 44.9, 46.9, 46.9, and 57.7 MeV fm^3 for the spline version.

Extrapolating the spline potential to the energies measured by Boschitz *et al.*[14] (31.8 and 41.0 MeV, respectively) leads to a nice semiquantitative agreement with the data as can be seen in Fig. 3; no attempt to fit these

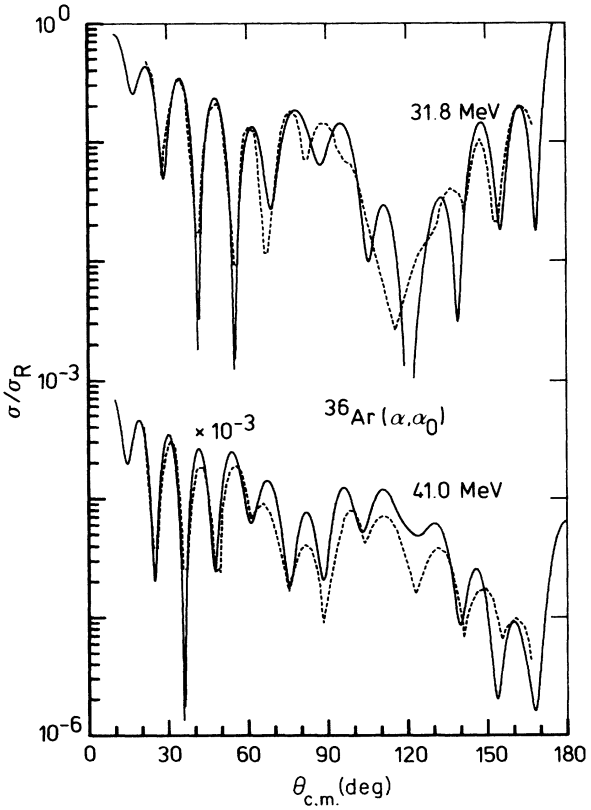

FIG. 3. Predictions of the spline potential (solid line) as compared with the experimental ^{36}Ar(α,α_0) data of Boschitz *et al.*[14] (dashed line) at 31.8 and 41.0 MeV incident energies.

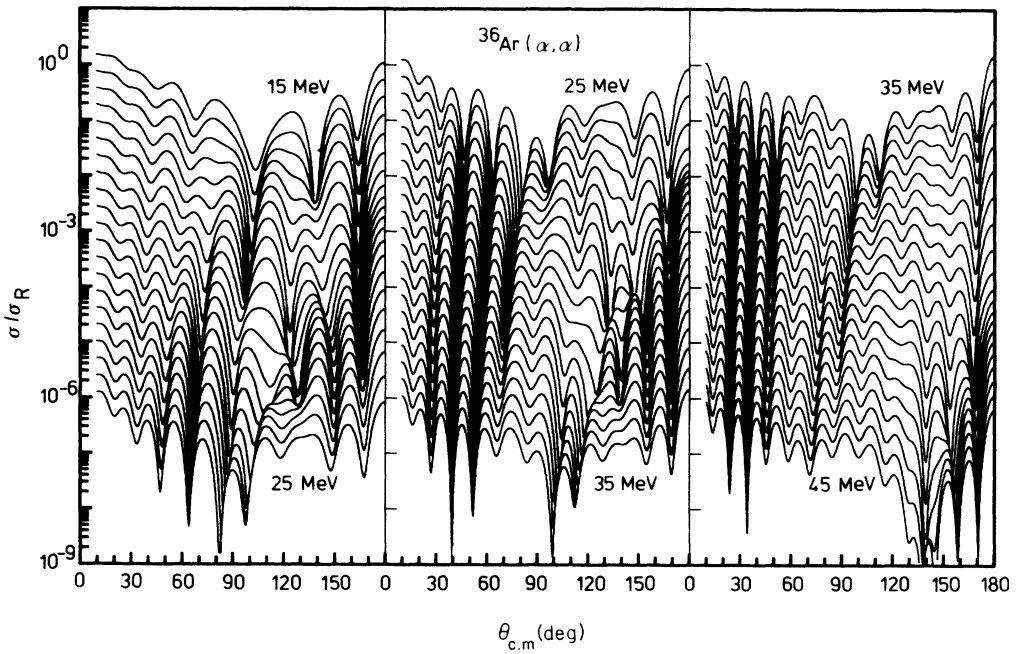

FIG. 4. Predictions of the spline potential between 15 and 45 MeV in 0.5 MeV steps; the energy behavior of the strengths λ and W_0 of the real and imaginary parts of the potential have been linearized from the values obtained at 18.0, 22.1, 24.1, and 29.2 MeV.

data was made since the numerical values of the latter were not available to the authors. It is seen that the characteristic, rapid change with energy displayed by the data in the 30–40 MeV range is very satisfactorily reproduced by the model. To make more apparent the intricacies of the energy behavior of the angular distributions, we present in Fig. 4 an "animated cartoon" view of the predictions of the spline potential between 15 and 45 MeV in 0.5 MeV steps.

To understand the origin of this very complicated energy behavior it is rewarding to decompose the optical-model amplitude into its barrier and internal wave contributions as defined by Brink and Takigawa;[19] as the original semiclassical scheme of Ref. 19 is untractable in the case of a spline potential, use was made of the alternative quantum method of Albinski and Michel[20] which has a wider range of applicability. The results of this decomposition, which we carried out at 18.0, 22.1, 24.1, and 29.2 MeV using the recipe of Ref. 20, are displayed in Fig. 5; as was found to be the case for the low-energy ^{40}Ca(α,α_0) data, the backward enhancement is seen to be mainly due to the internal wave contribution, that is, that part of the incident flux passing the barrier and reemerging after reflection at the most internal turning point, while as expected the forward angle region is dominated by the barrier wave contribution. As a result of a stronger absorption in the ^{36}Ar(α,α_0) case, however, the internal contribution is weaker than was the case for ^{40}Ca(α,α_0) scattering (the imaginary volume integral per nucleon pair was found to be 43.4 MeV fm^3 at 29 MeV in the model-independent analysis of Ref. 16, as compared to the value of 57.7 MeV fm^3 found here). A related difference be-

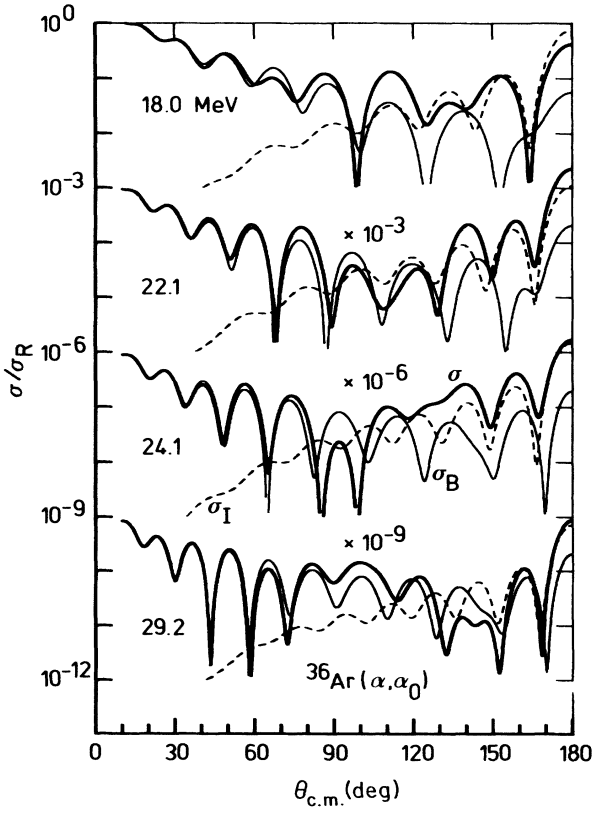

FIG. 5. Decomposition of the optical-model angular distribution $\sigma(\theta)$ (thick line) into its barrier (σ_B) (thin line) and internal wave (σ_I) (dashed line) contributions, normalized to Rutherford scattering (see text).

tween these two cases is that the interference between the barrier and internal amplitudes, which in the case of ^{40}Ca(α,α_0) scattering took place mainly in the mid-angle range, occurs now at more backward angles, in a region where the barrier contribution decreases relatively slowly with angle; as a result the interference pattern extends on a broader angular range, making the total (that is, barrier plus internal) cross section more sensitive to small changes of the incident energy—or of the optical-model parameters. This enhanced sensitivity explains why it is comparatively difficult to obtain as precise an agreement with the data as was the case for the $\alpha+^{40}$Ca system,[16,21] particularly in this broad angular region of strong interference.

III. BOUND AND QUASIBOUND STATES SUPPORTED BY THE POTENTIAL

In the spirit of an orthogonality condition model (OCM)-type interpretation[22] we are led to associate some of the states supported by these potentials with α-particle cluster states of the unified system. This approach is known to give a nice account of many properties of these states in ^{20}Ne and ^{44}Ti, such as their spins and excitation energies, spectroscopic factors and widths, and intraband transition rates.[2,23] It can be considered as an extension of the local potential model (LPM) initially proposed by Buck, Dover, and Vary[24] to describe the cluster state properties of nuclei of the $A \simeq 16$ region. An obvious advantage of the present approach is to provide a unified description within the same potential of the cluster state *and* of the scattering properties of the system up to high positive energies, in much the same way as the optical potential used to describe nucleon-nucleus scattering appears as the extension at positive energies of the shell-model potential describing the single-particle properties of the system at negative energies.[25]

In this picture, deeply bound states are interpreted as corresponding to the so-called forbidden states of the resonating group method[26] (RGM) and are therefore discarded. In the case of doubly closed shell partners, and in the limit where both are described by harmonic oscillator wave functions with equal oscillator parameters, these states satisfy the so-called Wildermuth condition, that is $N \equiv 2n+l < N_{\text{crit}}$: their "principal" quantum number N, which is defined in terms of the number of radial nodes n of the relative motion wave function with angular momentum l, must be less than some critical number N_{crit} (which is equal to 8 for the $\alpha+^{16}$O system and to 12 for $\alpha+^{40}$Ca). States with higher N values are considered as physical; they are found to group into quasirotational bands of constant N, which are associated with physical cluster states.

In the case of a non-closed-shell target as ^{36}Ar the Wildermuth condition cannot be stated so simply since in this case the outer major shell is not completely filled. However, if we restrict to the study of 4p-4h states of the unified system (^{40}Ca) we are led to impose the same constraint $N \geq 12$ to the physical states bound by the potential. Some of the states with $N < 12$, which are not completely forbidden, are expected to carry part of the strength of physical states with a different structure like, e.g., the ^{40}Ca ground state;[27] yet as the model space available for describing these states is clearly inadequate they will not be considered further.

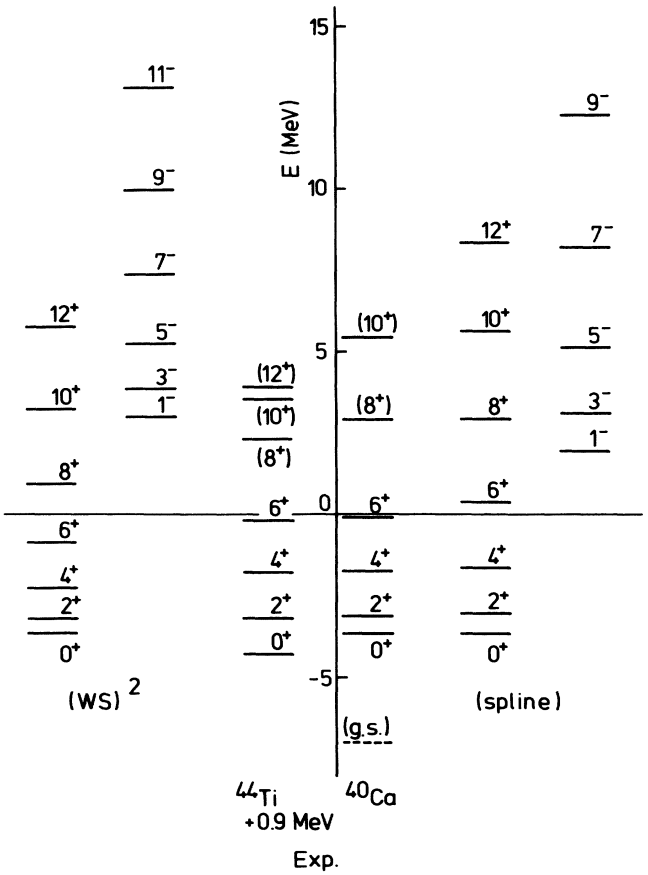

FIG. 6. States of the $N=12$ and $N=13$ quasirotational bands calculated with the Woods-Saxon squared potential (left) and the spline potential (right). Experimental candidates of the deformed positive-parity band built on the $J^\pi=0^+$, $E_x=3.35$ MeV state in ^{40}Ca, and the ^{44}Ti ground state band (shifted by 0.9 MeV) (center).

States with $N \geq 12$ were thus calculated using the real parts of the two optical potentials defined in Sec. II. In the case of the Woods-Saxon squared potential of Eqs. (1) and (2), a slight renormalization of the potential strength to $V_0=181.9$ MeV brings the $N=12$, $l=0$ state at the energy of the $J^\pi=0^+$, $E_x=3.35$ MeV 4p-4h bandhead (the $V_0=185$ MeV potential overbinds this state by some 2 MeV); similarly we used the spline potential with $\lambda=0.997$ to calculate these states. The resulting spectra are displayed in Fig. 6, together with the experimental candidates of the positive-parity band built on the deformed $J^\pi=0^+$, $E_x=3.35$ MeV state.[28,29] The spectra obtained with these two potentials are seen to be in essential agreement with each other; the two theoretical $N=12$ bands agree well with the experimental candidates, though the Woods-Saxon squared $N=12$ band appears somewhat too compressed with respect to the experimental levels. Also presented in the same figure is the ^{44}Ti ground state band, of which the ^{40}Ca positive-

TABLE I. Calculated rms radii and quadrupole transition probabilities for the states of the ^{40}Ca $N=12$ band, and experimental transition rates within the ^{40}Ca 4p-4h deformed band (Ref. 35). Calculations were performed using the Woods-Saxon squared (left columns) and the spline (right columns) potentials, respectively; the second column lists the normalization constants of the spline potential used to locate each level at the experimental energy (the same value of λ was used for $J^\pi=10^+$ and 12^+ since there is to date no experimental $J^\pi=12^+$ candidate).

		$\langle R^2\rangle^{1/2}$ (fm)		$B(E2)(J\to J-2)$ (e^2fm^4) This work		
J^π	λ					Exp.
0^+	0.997	4.52	4.56			
2^+	0.998	4.49	4.51	105	109	250±35
4^+	0.998	4.42	4.40	138	140	535±110
6^+	1.004	4.30	4.17	129	121	136^{+72}_{-36}
8^+	0.998	4.15	3.94	103	90	
10^+	1.000	3.98	3.69	70	54	
12^+	1.000	3.79	3.45	34	23	

parity band under discussion is thought to be the weak coupling partner; these two bands are very similar at low spin, except for the 0^+-2^+ spacing, the smaller value of which in ^{40}Ca has been interpreted in terms of mixing with the ^{40}Ca ground state through 2p-2h components.[29]

Previous investigations of this band within the LPM approach had been carried out by Pal and Lovas,[30] and more recently by Merchant[31,32] who used a local potential essentially similar to that of Ref. 30. A very good agreement with the experimental data was achieved in these studies, at the expense, however, of using a potential whose properties were not tested against the scattering properties of the $\alpha+^{36}$Ar system, and which turns out to disagree in the tail region with potentials compatible with the scattering data.[33] A similar potential used by the same authors to describe the α-cluster structure in ^{44}Ti (Ref. 31) has recently been revealed to be unrealistic in the tail region with respect to the predictions of folding model calculations using reasonable effective interactions: These calculations[34] confirm the essential features of the phenomenological $\alpha+^{40}$Ca potential used in Ref. 2 to describe the bound, quasibound, and scattering properties of the $\alpha+^{40}$Ca system.

We have also calculated the rms intercluster distance $\langle R^2\rangle^{1/2}$ and the $B(E2)$ intraband transition probabilities of these states using the Woods-Saxon squared potential and the spline potential, the normalization constant λ of which was finely tuned to locate each state at the correct experimental energy; these are presented in Table I together with the experimental data.[35] In contrast with the case of ^{44}Ti, where the local potential model calculations provide a nice description of experiment without having to introduce additional effective charges[2] the calculation underestimates the $2^+\to0^+$ and the $4^+\to2^+$ transition rates by a factor of 2 to 3, while the $6^+\to4^+$ transition is described more satisfactorily. The LPM calculations of Refs. 30–32 reproduce the first two transition rates better, but as explained in the preceding paragraph this is directly connected with the unphysically long tail of the potential used, which makes the wave functions extend farther out in the surface region than those of our calculations.

Examination of our calculated rms radii shows that the cluster character of these states, which is already relatively weak at low spin (the rms intercluster distance obtained for the $J^\pi=0^+$ state should be compared to the sum of the ^{4}He and ^{36}Ar rms charge radii,[36,37] which amounts to 5.00 fm), decreases with increasing spin because of an antistretching effect similar to that evidenced by the ^{44}Ti ground state band.[2] The underestimation of the $2^+\to0^+$ and $4^+\to2^+$ transition rates seems to indicate, however, that our model somewhat underestimates the degree of clustering of these states, and indeed the rms charge radius of the $J^\pi=0^+$ state, which is given by

$$\langle r^2\rangle_{\rm ch}=\tfrac{9}{100}\langle R^2\rangle+\tfrac{1}{10}\langle r^2\rangle_{\rm ch,He}+\tfrac{9}{10}\langle r^2\rangle_{\rm ch,Ar}\ , \qquad (3)$$

where we have taken $\langle r^2\rangle^{1/2}_{\rm ch,He}=1.674$ fm (Ref. 36) and $\langle r^2\rangle^{1/2}_{\rm ch,Ar}=3.33$ fm (Ref. 37), amounts to 3.48 fm, which coincides with the experimental ^{40}Ca ground state rms charge radius of 3.48 fm,[36] whereas we would expect a substantially larger rms radius for this 4p-4h, deformed state. Taking explicitly into account the coupling to the excitation of the 2^+ and 4^+ states of the ^{36}Ar core could possibly alleviate this problem, though most probably by only a modest amount.[32]

The potential supports another positive-parity band of states with $N=14$, which is the analog of the well-known $N=10$ "higher nodal" positive-parity band based on the $J^\pi=0^+_4$, $E_x\simeq8.7$ MeV state in ^{20}Ne,[38] and of the $N=14$ band in ^{44}Ti, which starts at $E_\alpha\simeq7$ MeV (Ref. 2) and was shown[6] to be responsible for the broad oscillations seen at low energy in the experimental $\alpha+^{40}$Ca fusion excitation function. Measurement of the $\alpha+^{36}$Ar fusion excitation function in a similar energy range could provide a direct evidence for the existence of this positive-parity excited band.

Additional bands of positive and negative parity with $N\geq15$, composed of very broad, overlapping states, can be traced at higher excitation energy. They play an important role in the building up of the backward rise at low scattering energies. As the mechanism of the enhancement observed here is closely similar to that displayed by the $\alpha+^{40}$Ca system[2] no discussion of these higher-lying bands will be reported here.

More interesting to investigate are the properties of the

TABLE II. Energies, widths, and dimensionless reduced widths of the states of the $N=13$ negative-parity band, calculated with the Woods-Saxon squared (left columns) and the spline (right columns) real potentials ($V_0=181.9$ MeV and $\lambda=0.997$, respectively).

J^π	$E_{r,c.m.}$ (MeV)		$\Gamma_{c.m.}$ (keV)		θ_l^2 (%) ($a=7.25$ fm)	
1^-	2.95	1.82	0.05	$\ll 0.001$	25	~ 25
3^-	3.78	2.92	0.40	0.006	22	23
5^-	5.23	4.96	2.4	1.10	19	16
7^-	7.29	8.00	4.0	15.8	10	15
9^-	9.92	12.1	3.3	46.8	4.3	11
11^-	13.1	16.6	1.2	26.1	1.2	3.3
13^-	16.6	21.0	0.14	2.2	0.13	0.26

$N=13$ negative-parity band, which is the analog of the famous $N=9$ "inversion-doublet" band in ^{20}Ne,[1] and which we predict to start a few MeV above the $\alpha+^{36}$Ar threshold (Fig. 6). Whereas the ^{20}Ne ground state band is composed of states with restricted cluster character, which can be described to a good approximation in conventional shell-model calculations, it is known that the states of this negative-parity band are considerably more clusterlike, with enhanced intraband transition probabilities (in fact only the $3^-\rightarrow 1^-$ transition is known experimentally[39]) and larger rms intercluster distances. In the case of the $\alpha+^{40}$Ca system, previous calculations of the present authors predicted the $N=13$ band to start just above the $\alpha+^{40}$Ca threshold, and the low-spin members to display appreciable cluster character. It was pointed out in that work[2] that a key issue for confirming the persistency of α-particle clustering in the fp-shell region would be the observation of these states, which have up to now no experimental counterpart, in, e.g., α-particle transfer experiments.

We want to stress here that the $\alpha+^{36}$Ar system could provide better prospects of observing these states experimentally. We have calculated the energy location and widths Γ_l of the states of this negative-parity band using the two potentials defined in Sec. II; their strength was fixed, according to the prescription stated above, to $V_0=181.9$ MeV and $\lambda=0.997$, respectively. These energies and absolute widths are reported in Table II; the widths are seen to range from a fraction of an eV to a few keV. We have deduced the corresponding dimensionless reduced widths θ_l^2, using the channel radius $a=7.25$ fm, obtained by scaling the value $a=7.50$ fm used in previous calculations of the $\alpha+^{40}$Ca system[2] according to an $A^{1/3}$ prescription; these are defined in terms of the Coulomb wave functions at the channel radius by the well-known relations of R-matrix theory:[40]

$$\Gamma_l=2P_l\gamma_l^2 , \tag{4.1}$$

$$P_l=ka/(F_l^2+G_l^2) , \tag{4.2}$$

$$\theta_l^2=\frac{2\mu a^2}{3\hbar^2}\gamma_l^2 , \tag{4.3}$$

where use was made of standard notations. The obtained values of θ_l^2 are also listed in Table II. Although the energy locations and spacings of the states predicted by the two potentials are somewhat different the dimensionless reduced widths are very similar for the first members of the band. Comparison with the dimensionless reduced widths obtained for the $\alpha+^{40}$Ca system[2] shows that the values obtained here are larger than the latter by more than 50%. The predicted degree of clustering of the "inversion-doublet" band thus appears to be higher in ^{40}Ca as compared to the ^{44}Ti case. As, in addition, the level density in ^{40}Ca is lower than in ^{44}Ti at comparable excitation energies because of the closed-shell nature of the former, we expect that the experimental identification of these states might be easier in the present case. Alpha-particle transfer experiments like[9] (^{6}Li,d) appear to be the most promising for investigating this problem. A few negative-parity candidates have been detected[41] below the $\alpha+^{36}$Ar threshold in the ^{36}Ar(^{6}Li,d)^{40}Ca reaction, but the lack of theoretical guidance at that time apparently prevented a more detailed investigation of these states. A careful study of the ^{40}Ca nucleus above $E_x\simeq 8$ MeV would be of great value to unravel its α-cluster spectroscopy; measurement of d-α angular correlations in the (^{6}Li,d) reaction could make possible a more unambiguous determination of the spins of possible candidates.

We end this section by presenting in Table III the rms radii and intraband quadrupole transition probabilities for the states of the $N=13$ band, calculated using the Woods-Saxon squared potential and the spline potential with $\lambda=0.997$. Examination of these quantities confirms the enhanced α-cluster character of the low-spin members of this band with respect to those of the $N=12$ band; indeed the rms intercluster distance is now comparable to the sum of the radii of the free cluster and core, and the $B(E2)$'s are substantially enhanced with respect

TABLE III. Rms radii and quadrupole transition probabilities for the states of the ^{40}Ca $N=13$ band, calculated with the Woods-Saxon squared (left columns) and with the spline ($\lambda=0.997$) potentials, respectively.

J^π	$\langle R^2\rangle^{1/2}$ (fm)		$B(E2)(J\rightarrow J-2)$ (e^2fm^4)	
1^-	5.36	5.38		
3^-	5.29	5.37	258	274
5^-	5.15	5.32	271	309
7^-	4.93	5.19	234	298
9^-	4.65	4.88	174	240
11^-	4.34	4.29	107	129
13^-	4.03	3.68	49	35

to those calculated in the $N=12$ case. The low-spin members of the $N=14$ band, which manifest themselves as broad resonances with widths of the order of 1 MeV, have even stronger cluster character since their reduced widths are of the order of the Wigner limit.

IV. ALPHA-CLUSTER SPECTROSCOPY AROUND THE *sd*-SHELL CLOSURE

We briefly discuss the possible extensions of the local potential picture for investigating α-particle structure in systems close to the $\alpha+^{36}$Ar and $\alpha+^{40}$Ca systems which we considered here and in Ref. 2, respectively. Because there exists a vast literature relevant to this field and not a few nuclei will be included in the discussion, an extensive coverage of this point goes obviously beyond the scope of this paper: We rather intend to draw a few guidelines to possible extensions of this work, basing ourselves on a restricted set of pertinent references to select plausible candidates to such a description.

The coexistence of spherically symmetric states with simple shell-model structure, and of deformed rotational states at low excitation energy, is a well-documented feature in the $A\simeq 40$ mass region.[7,8,42–44] It has often been described by mixing spherical shell-model wave functions with Nilsson model deformed components, or within a weak coupling picture where shell-model wave functions are mixed with particle-hole excitations of the core. As was found to be the case for the $\alpha+^{36}$Ar system, the local potential model could provide an interesting alternative to a systematic description of these states in terms of α-particle clustering.

A. The ^{41}Ca, ^{41}Sc, ^{42}Ca, ^{43}Sc, and ^{43}Ti nuclei

We first concentrate on systems made up of a nonclosed-shell core with neutron and proton numbers intermediate between those of ^{36}Ar and ^{40}Ca. In a weak coupling picture where the ^{44}Ti ground state band is coupled to the ground state of the core we expect the LPM to be able to describe excited states of the unified system having 4p-mh structure, where m is the number of holes in the core. These states would appear as intruder states in $(fp)^n$ shell-model calculations.[45] This type of description is expected to work best if the excitation energy of the first excited state of the core is not too low, and if the candidate cluster states are not too far from the α-particle threshold ("threshold rule"[46]). The best candidate nuclei to such a description appear to be ^{41}Ca, ^{41}Sc, ^{42}Ca, ^{43}Sc, and ^{43}Ti; for these five systems the excitation energy of the first excited state of the core is larger than 1 MeV,[47] and there exist enough data to identify plausible candidates. We note that α-particle structure in ^{42}Ca and ^{43}Sc has recently been investigated by Merchant[31,48] within a local potential approach, without reference, however, to the description of the scattering regime.

Ideally to comply with our philosophy the local potential used to describe these states should be derived from the real part of an optical-model potential describing low-energy $\alpha+$ core scattering data—or at least be justified in terms of such a potential. This condition can, however, be partly circumvented in the range of masses studied here since the real parts of the optical potentials describing the two extreme systems ($\alpha+^{36}$Ar and $\alpha+^{40}$Ca) are very similar. Moreover, there are convincing hints that potentials describing intermediate-mass systems are very close to those used for $\alpha+^{36}$Ar and $\alpha+^{40}$Ca. Indeed the elastic scattering $\alpha+^{39}$K data of Bobrowska *et al.*[49] between 22.1 and 28.2 MeV are nearly identical to the $\alpha+^{40}$Ca data at comparable energies, and the corresponding optical-model potentials must therefore be very similar; this has recently been confirmed by an analysis of these data by Ohkubo.[50] In addition, the only available $\alpha+^{38}$Ar elastic scattering angular distribution measured at $E_\alpha=24$ MeV (Ref. 51) is very similar to the $\alpha+^{36}$Ar angular distribution at the same energy (except for slightly lower cross sections at large angles), implying again that a very similar optical potential (with possibly slightly stronger absorption) should describe these data. Since ^{37}Ar and ^{37}K are instable isotopes, no elastic scattering data are available for these systems.

In ^{42}Ca there exist 4p-2h core-excited candidates, the most often quoted being the $J^\pi=0^+$, $E_x=1.84$ MeV and $J^\pi=2^+$, $E_x=2.42$ MeV states;[7,8,42] there exists also an intruder $J^\pi=4^+$ state at $E_x=3.25$ MeV, which has been associated with these two states in a common deformed rotational band.[52] States with $J^\pi=6^+$, $E_x=4.715$ MeV and $J^\pi=8^+$, $E_x=6.633$ MeV have subsequently been identified by Betz *et al.*[53] and associated with the same band; indeed the measured $B(E2)$ intraband transition rates within this band show strong enhancement, and take on values comparable to those found within the 4p-4h band in ^{40}Ca. The similarity of the $\alpha+^{38}$Ar potential with the $\alpha+^{36}$Ar and $\alpha+^{40}$Ca interactions implies similar intraband transition rates, which are thus expected to take values comparable to those obtained for the ^{40}Ca and ^{44}Ti systems, that is $B(E2)$'s of the order of 10 to 20 Weisskopf units (W.u.) for the low-spin transitions; as was found to be the case for the $\alpha+^{36}$Ar system, these estimates are on the low side since $B(E2)$'s of 57 ± 20, 50^{+35}_{-16}, and 63^{+47}_{-17} W.u. have been reported for the $4^+\rightarrow2^+$, $6^+\rightarrow4^+$, and $8^+\rightarrow6^+$ transitions, respectively.[53,54] The similarly of the potentials also implies the existence of an excited negative-parity band with $N=13$, starting some 5 MeV above the bandhead of the α-cluster positive-parity band; if we stick to the choice of the $J^\pi=0^+$, $E_x=1.84$ MeV state as the experimental candidate for the positive-parity bandhead, we are thus led to predict the existence of a negative-parity band of states starting with $J^\pi=1^-$ around $E_x\simeq7$ MeV (that is, very near the $\alpha+^{38}$Ar threshold), with strong α-cluster character.

In the odd-even ^{41}Ca, ^{41}Sc, ^{43}Sc, and ^{43}Ti nuclei the possible 4p-mh intruder-state candidates are not difficult to pinpoint since, contrary to the $(fp)^n$ shell-model states, they have positive parity. Coupling of the $N=12$ cluster-core relative motion angular momentum with the spin of the core leads to the prediction of a positive-parity, half-integer spin band of states, the bandhead of which should have the spin of the core; for the systems investigated here the core has $J^\pi=\frac{3}{2}^+$,[47] which should

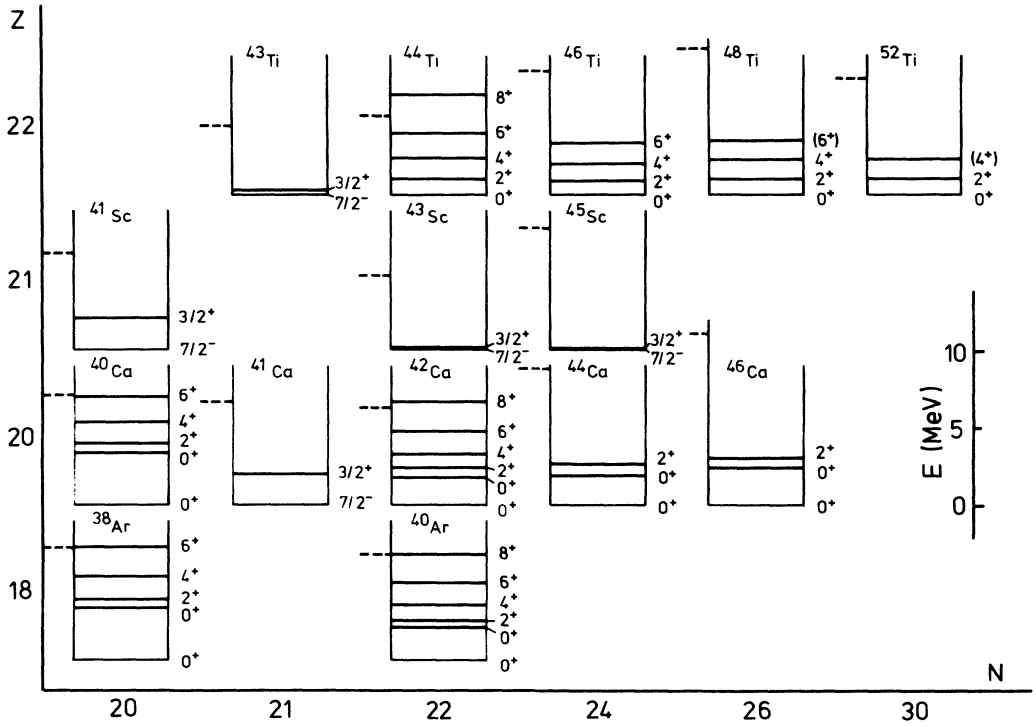

FIG. 7. Experimental α-cluster state candidates in the region of the *sd*-shell closure (see text), represented in the (N,Z) plane (note the discontinuities in the scales); the dashed line on the left side of each spectrum indicates the α-particle threshold. For odd-A nuclei only the first state of the band ($\frac{3}{2}^+$) has been shown for clarity.

thus also be the quantum numbers of the bandhead of the first cluster band. Coupling the $l=2,4,\ldots$ orbital angular momenta with the $\frac{3}{2}$ spin of the core results in quadruplets whose degeneracy is expected to be lifted by possible noncentral components of the cluster-core interaction. However since a good fit to the $\alpha+^{39}$K scattering data does not require the explicit introduction of such a component,[50] it is expected to be weak and not to ruin the identification of these quadruplets, at least in the case of the ^{43}Sc nucleus. In his very detailed study of the ^{43}Sc cluster spectroscopy, Merchant introduced such a tensor component in his $\alpha-^{39}$K interaction to reproduce in a quantitative way the splitting of the quadruplets; moreover he also introduced the possibility of an excitation of the ^{39}K core to its first $J^\pi=\frac{1}{2}^+$ excited state.

All four nuclei under investigation indeed possess a low-lying $J^\pi=\frac{3}{2}^+$ intruder state at low energy, which is in addition the first positive-parity state of their spectrum: This state falls at $E_x=2.01$, 2.10, 0.16, and 0.31 MeV in ^{41}Ca, ^{41}Sc, ^{43}Sc, and ^{43}Ti, respectively.[47,55] It is followed by several positive-parity states with quantum numbers corresponding to those expected for the first quadruplets, although some experimental candidates appear to be missing, particularly in the case of ^{41}Sc; the centroids of these quadruplets have energies with respect to the bandhead comparable to those of the first excited states in the $N=12$ α-cluster band in ^{40}Ca and ^{44}Ti. The candidates to such a local potential model description are plotted in Fig. 7, where we have also indicated the position of the α-particle threshold. We note that the ^{43}Sc experimental positive-parity spin sequence has been interpreted in terms of two rotational bands built on deformed intrinsic states with $K^\pi=\frac{3}{2}^+$ and $K^\pi=\frac{1}{2}^+$.[56–58]

B. The ^{38}Ar and ^{40}Ar nuclei

We can extend these considerations to the ^{38}Ar and ^{40}Ar systems where coexistence of spherical and deformed states has also been reported.[54,59] In this case the cores to be considered, that is ^{34}S and ^{36}S, are quite acceptable since the excitation energy of their first excited states are 2.13 and 3.29 MeV, respectively.[47] To our knowledge no optical-model analysis has been reported for these systems (α-particle scattering from the rare ^{36}S isotope has not been measured), and we can only make plausible extrapolations of the results obtained for the neighboring $\alpha+^{36}$Ar system. We note in this respect that the ^{34}S(α,α_0) angular distribution measured at $E_\alpha=24$ MeV is very similar to that of ^{36}Ar(α,α_0) at the same energy,[51] with a comparable backangle enhancement, pointing to the possibility of describing these data with similar optical potentials. In ^{38}Ar the candidates to our description are the $J^\pi=0^+$, $E_x=3.38$ MeV; $J^\pi=2^+$, $E_x=3.94$ MeV; $J^\pi=4^+$, $E_x=5.35$ MeV; $J^\pi=(6^+)$, $E_x=7.29$ MeV; and $J^\pi=(8^+)$, $E_x=9.34$ MeV states, which have been shown to have predominantly 4p-6h structure.[60] In ^{40}Ar the $J^\pi=0^+$, $E_x=2.12$ MeV; $J^\pi=2^+$, $E_x=2.52$ MeV; $J^\pi=4^+$, $E_x=3.51$ MeV; $J^\pi=6^+$, $E_x=4.96$ MeV; and $J^\pi=(8^+)$, $E_x=6.81$ MeV states[54] are obvious candidates; however, these states, which in Ref. 54 are considered to have two-hole structure, would more naturally be interpreted in our description as being of 4p-4h nature.

These bands are similar to the 4p-2h band in ^{42}Ca (Fig. 7), and the experimentally known intraband transition rates take on comparable, enhanced values.[54]

C. The ^{44}Ca, ^{45}Sc, and ^{46}Ca nuclei

We next shift to a few systems with a non-closed-shell core, but with a few extra protons or neutrons outside the core where our description could also reveal meaningful: We will restrict here to the ^{44}Ca, ^{45}Sc, and ^{46}Ca systems. In ^{44}Ca and ^{46}Ca it is well known that $(fp)^n$ shell-model calculations cannot account for the second 0^+ and 2^+ states of the spectrum, and these states are therefore considered to be predominantly core excited.[45,61] The excitation energies of these two-hole 0^+ states in ^{44}Ca and ^{46}Ca are similar to that of the 4p-2h 0_2^+ state in ^{42}Ca, since they amount to 1.89 and 2.42 MeV, respectively [$E_x(0_2^+)=1.84$ MeV in ^{42}Ca]. We note, however, that core deformation has been found to be substantially smaller in ^{46}Ca than in its neighbors ^{42,44}Ca,[62] and indeed $(fp)^n$ shell-model calculations do not suffer so much from the presence of intruders.[45] In the ^{45}Sc system where the ^{41}K core has $J^\pi=\frac{3}{2}^+$, the first 5p-1h state, which is nearly degenerate with the $J^\pi=\frac{7}{2}^-$ ground state, has $J^\pi=\frac{3}{2}^+$, and is followed by positive-parity states with the quantum numbers of quadruplets similar to those discussed in connection with ^{41}Sc, ^{41}Ca, and ^{43}Sc; in the more conventional approach, coexistence with deformed states is discussed in terms of two rotational bands built on intrinsic $K^\pi=\frac{3}{2}^+$ and $K^\pi=\frac{1}{2}^+$ states.[56,58,63] Among the three systems considered in this paragraph, only $\alpha+^{40}$Ar scattering has been investigated experimentally by Gaul *et al.*[13] between 22 and 29 MeV. Absorption is much stronger than is the case in $\alpha+^{36}$Ar and $\alpha+^{40}$Ca, and the anomalous features of the backangle angular distributions of the latter are largely absent; although the real part of the potential is not so well determined in this case, it has proved possible to fit the data using a potential with a real part very similar to that used for the $\alpha+^{40}$Ca system.[16]

D. The ^{46}Ti, ^{48}Ti, and ^{52}Ti nuclei

We end this section with a brief description of a few systems with a closed-shell core and several neutrons outside the core, i.e., the Ti isotopes with $A=46$, 48, and 52. Elastic α-particle scattering from ^{42}Ca, ^{44}Ca, and ^{48}Ca has been investigated experimentally, from low[13] ($E_\alpha\simeq 25$ MeV) to high[64] ($E_\alpha=104$ MeV) incident energies. While ^{44}Ca(α,α_0) scattering is characterized by strong absorption at low energy, ^{42}Ca and ^{48}Ca lead to angular distributions intermediate in character between the backangle-enhanced ones of ^{36}Ar, ^{40}Ca(α,α_0) and the diffraction-like angular distributions of ^{40}Ar, ^{44}Ca(α,α_0).[13] It has proved possible to fit precisely the low-energy data using optical potentials with real parts very similar to those used for ^{40}Ca(α,α_0) scattering;[16] a similar result is obtained in the model-independent analysis of Gils *et al.*[64] at $E_\alpha=104$ MeV incident energy. The most conspicuous feature of the extracted real potentials is a slow systematic increase of their rms radii with mass number. These results are consistent with the calculations of Wintgen *et al.*,[65] where the local $\alpha-^{40,42,44,48}$Ca potentials which are derived from their microscopic generator coordinate method energy surfaces are found to depend smoothly on the mass of the target nucleus. In this case the absence of holes in the core leads us to put the states of the $N=12$ positive-parity band in correspondence with the experimental states of the ^{46,48,52}Ti ground state bands. In these nuclei the $J^\pi=2_1^+$ and 4_1^+ states are located at nearly identical excitation energies as in ^{44}Ti. Because of the threshold rule the cluster character of these states is expected to be weak in ^{48}Ti (and in ^{50}Ti which is not discussed here), but could be instrumental in explaining the rather high values found for the intraband $B(E2)$'s for the low-spin states in ^{46}Ti.[66] Also the discussion of the intraband transition rates and quadrupole moments of these nuclei in terms of α-particle clustering could be an interesting alternative to the more usual interpretations relying on particle-hole excitations from the $f_{7/2}$ shell to the upper part of the fp shell.

E. Hypothetical negative-parity band around $A=40$

An important aspect of the picture we have developed in this section is the prediction of the systematic occurrence in the range of masses discussed here of a negative-parity band of states with $N=13$, starting around the α-particle threshold. This band should be composed of states with more distinct cluster character, although this character could vary significantly from one system to the other according to the position of these states with respect to the threshold. Also the observability of these states is expected to depend sensitively on the density of states around the threshold, which makes odd-A nuclei unlikely candidates to such an observation since in addition coupling of the spin of the core with the cluster-core relative angular momentum will split these states into several components. In these conditions the best candidates for the observation of these states appear to be ^{38}Ar, ^{40}Ar, and ^{42}Ca—in addition to the ^{40}Ca system discussed in Sec. III (and the ^{44}Ti system discussed in Ref. 2)—and accordingly α-particle transfer experiments on the ^{34}S, ^{36}S, ^{36}Ar, and ^{38}Ar nuclei could be worth investigating, although all of these targets turn out unfortunately to be rather rare isotopes.

V. SUMMARY AND CONCLUSIONS

In this paper we have subjected the existing low-energy ^{36}Ar (α,α_0) scattering data to an optical-model analysis, starting from the unique optical potential describing the ^{40}Ca(α,α_0) data on broad energy and angular ranges. Both Woods-Saxon squared and model-independent form factors were used for parametrizing the real part of the potential; it proved possible to describe the complicated evolution of the data with energy—including the enhancement observed at back angles—using energy-independent real and imaginary form factors. To understand better the origin of the intricate energy behavior of the data we have decomposed the optical-model scatter-

ing amplitude into its barrier and internal wave contributions.

Bound and quasibound states supported by the real part of the extracted potential were then calculated in the spirit of an OCM-type interpretation where the deeply-bound states with $N<12$ are discarded, since they are supposed to simulate the so-called forbidden states of the RGM. States with $N=12$ were found to group into a (positive-parity) quasirotational band agreeing well in energy with the well-known 4p-4h deformed band in ^{40}Ca, built on the $J^{\pi}=0^{+}$, $E_x=3.35$ MeV deformed state. The calculated rms intercluster distances are smaller than the sum of the free cluster and core radii and decrease with increasing spin (antistretching effect), which indicates that this band has a relatively weak cluster character. However, our calculations underestimate the $4^{+}\rightarrow 2^{+}$ and $2^{+}\rightarrow 0^{+}$ $B(E2)$ intraband transition rates, indicating that our model probably underestimates somewhat the degree of clustering of these states. The potential supports an excited $N=14$ positive-parity band of states which could be detected by a measurement of the $\alpha+^{36}$Ar fusion excitation function, and broad, overlapping states with $N\geq 15$ which contribute to the backangle enhancement observed in the scattering data at low energy. It supports in addition a $N=13$ negative-parity band of states, with a substantial cluster character which could be detected by investigating α-particle transfer on the ^{36}Ar nucleus; it has been pointed out that the $\alpha+^{36}$Ar system could provide better prospects of observing these states than the $\alpha+^{40}$Ca system discussed in Ref. 2, because of larger reduced widths and of the lower level density in ^{40}Ca as compared to that in ^{44}Ti.

Finally we have examined in an exploratory discussion the possibility of extending this type of approach to neighboring systems ranging from ^{38}Ar to ^{52}Ti, by enumerating plausible candidate states in these systems while keeping contact with the few existing α-particle scattering data on the relevant core nuclei. Although somewhat speculative, this discussion indicates that investigating the coexistence of spherically symmetric and deformed states in the $A\simeq 40$ mass region in terms of α-particle clustering could prove rewarding. If a slowly varying α-core potential can indeed be defined meaningfully around the *sd*-shell closure region, an important consequence of our picture is the prediction of the systematic occurrence in this range of masses of a negative-parity band of states with distinct cluster character, starting around the α-particle threshold.

ACKNOWLEDGMENTS

F.M. acknowledges the Research Institute for Fundamental Physics, Kyoto University, for inviting him to Japan and for financial support, and Kochi Women's University, where part of this work was completed, for their kind hospitality. F.M. and G.R. are grateful to Professor R. Ceuleneer for his interest during the course of this work. S.O. thanks Miss K. Umehara for collaboration in the initial stage of this work, and Professor Y. Tanaka and the members of the research project on "Molecule-like structure in *fp*-shell, medium-weight and heavy nuclei," organized by the Research Institute for Fundamental Physics, Kyoto University, for valuable discussions. S.O. has been supported by a Grant-in-Aid for scientific research of the Ministry of Education, Science and Culture in 1987–1989 (Grant No. 62540212).

[1]Y. Fujiwara, H. Horiuchi, K. Ikeda, M. Kamimura, K. Katō, Y. Suzuki, and E. Uegaki, Suppl. Prog. Theor. Phys. **68**, 29 (1980); H. Furutani, H. Kanada, T. Kaneko, S. Nagata, H. Nishioka, S. Okabe, S. Saito, T. Sakuda, and M. Seya, *ibid.* **68**, 193 (1980), and references therein.

[2]F. Michel, G. Reidemeister, and S. Ohkubo, Phys. Rev. Lett. **57**, 1215 (1986); Phys. Rev. C **37**, 292 (1988).

[3]Th. Delbar, Gh. Grégoire, G. Paic, R. Ceuleneer, F. Michel, R. Vanderpoorten, A. Budzanowski, H. Dabrowski, L. Freindl, K. Grotowski, S. Micek, R. Planeta, A. Strzalkowski, and K. A. Eberhard, Phys. Rev. C **18**, 1237 (1978).

[4]S. Ohkubo, Phys. Rev. C **38**, 2377 (1988).

[5]T. Wada and H. Horiuchi, Phys. Rev. C **38**, 2063 (1988).

[6]F. Michel, G. Reidemeister, and S. Ohkubo, Phys. Rev. C **34**, 1248 (1986).

[7]W. J. Gerace and A. M. Green, Nucl. Phys. **A93**, 110 (1967).

[8]P. Federman and S. Pittel, Phys. Rev. **186**, 1106 (1969).

[9]H. W. Fulbright, Annu. Rev. Nucl. Part. Sci. **29**, 161 (1979).

[10]R. K. Sheline and K. Wildermuth, Nucl. Phys. **21**, 196 (1960).

[11]F. Michel and G. Reidemeister, in Proceedings of the International Conference on Interactions and Structures in Nuclei, Brighton, 1987, edited by R. J. Blin-Stoyle and W. D. Hamilton (unpublished).

[12]S. Ohkubo and K. Umehara, Prog. Theor. Phys. **80**, 598 (1988).

[13]G. Gaul, H. Lüdecke, R. Santo, H. Schmeing, and R. Stock, Nucl. Phys. **A137**, 177 (1969).

[14]E. T. Boschitz, J. S. Vincent, R. W. Bercaw, and J. R. Priest, Phys. Rev. Lett. **13**, 442 (1964).

[15]W. J. Wallace, K. R. Knuth, and R. H. Davis, Phys. Rev. C **2**, 1738 (1970).

[16]F. Michel and R. Vanderpoorten, Phys. Lett. **82B**, 183 (1979).

[17]H. P. Gubler, U. Kiebele, H. O. Meyer, G. R. Plattner, and I. Sick, Nucl. Phys. **A351**, 29 (1981).

[18]P. J. Ellis, Z. El-Itaoui, M. A. Franey, and B. A. Mughrabi, Nucl. Phys. **A458**, 269 (1986).

[19]D. M. Brink and N. Takigawa, Nucl. Phys. **A279**, 159 (1977).

[20]J. Albinski and F. Michel, Phys. Rev. C **25**, 213 (1982).

[21]F. Michel and G. Reidemeister, Phys. Rev. C **29**, 1928 (1984).

[22]S. Saito, Prog. Theor. Phys. **41**, 705 (1969).

[23]F. Michel, J. Albinski, P. Belery, Th. Delbar, Gh. Grégoire, B. Tasiaux, and G. Reidemeister, Phys. Rev. C **28**, 1904 (1983).

[24]B. Buck, C. B. Dover, and J. P. Vary, Phys. Rev. C **11**, 1803 (1975).

[25]P. E. Hodgson, in *Proceedings of the Fifth International Conference on Clustering Aspects in Nuclear and Subnuclear Systems, Kyoto, 1988,* edited by K. Ikeda, K. Katori, and Y. Suzuki [J. Phys. Soc. Jpn. Suppl. **58**, 755 (1989)].

[26]K. Wildermuth and Y. C. Tang, *A Unified Theory of the Nucleus* (Vieweg, Braunschweig, 1977).

[27]T. Ogawa, Y. Suzuki, and K. Ikeda, Prog. Theor. Phys. **57**, 1072 (1977).

[28]P. M. Endt and C. Van der Leun, Nucl. Phys. **A310**, 1 (1978); P. Braun-Munzinger, C. K. Gelbke, N. Grama, H. Homeyer, E. Ridinger, and R. Stock, Phys. Rev. Lett. **29**, 1261 (1972).
[29]R. R. Betts, H. T. Fortune, J. N. Bishop, M. N. I. Al-Jadir, R. Middleton, Nucl. Phys. **A292**, 281 (1977).
[30]K. F. Pal and R. G. Lovas, Phys. Lett. **96B**, 19 (1980).
[31]A. C. Merchant, Phys. Rev. C **36**, 778 (1987).
[32]A. C. Merchant, Phys. Rev. C **37**, 414 (1988).
[33]S. Ohkubo, Phys. Rev. C **39**, 1186 (1989).
[34]A. C. Merchant, K. F. Pal, and P. E. Hodgson, J. Phys. G **15**, 601 (1989).
[35]J. R. MacDonald, D. H. Wilkinson, and D. E. Alburger, Phys. Rev. C **3**, 219 (1971); A. M. Nathan and J. J. Kolata, *ibid.* **14**, 171 (1976).
[36]R. C. Barrett and D. F. Jackson, *Nuclear Sizes and Structure* (Clarendon, Oxford, 1977).
[37]J. M. Finn, H. Crannel, P. L. Hallowell, J. T. O'Brien, and S. Penner, Nucl. Phys. **A274**, 28 (1976).
[38]F. Ajzenberg-Selove, Nucl. Phys. **A475**, 1 (1987).
[39]J. D. MacArthur, H. C. Evans, J. R. Leslie, and H.-B. Mak, Phys. Rev. C **22**, 356 (1980).
[40]A. M. Lane and R. G. Thomas, Rev. Mod. Phys. **30**, 257 (1958).
[41]H. T. Fortune, M. N. I. Al-Jadir, R. R. Betts, J. N. Bishop, and R. Middleton, Phys. Rev. C **19**, 756 (1979).
[42]B. H. Flowers and L. D. Skouras, Nucl. Phys. **A116**, 529 (1968); **136**, 353 (1969).
[43]A. P. Zuker, in *Proceedings of the Topical Conference on the Structure of* $1f_{7/2}$ *Nuclei, Legnaro, Italy, 1971,* edited by R. A. Ricci (Editrice Compositori, Bologna, 1971), p. 95.
[44]R. A. Ricci and P. R. Maurenzig, Riv. Nuovo Cimento **1**, 291 (1969).
[45]A. Poves and A. Zuker, Phys. Rep. **70**, 235 (1981).
[46]K. Ikeda, N. Takigawa, and H. Horiuchi, Prog. Theor. Phys. Suppl. **Extra Number**, 464 (1968).
[47]C. M. Lederer and V. S. Shirley, *Table of Isotopes,* Seventh Edition (Wiley, New York, 1978).
[48]A. C. Merchant, J. Phys. G **10**, 885 (1984).
[49]A. Bobrowska, A. Budzanowski, K. Grotowski, L. Jarczyk, S. Micek, K. Niewodniczanski, A, Strzalkowski, and Z. Wrobel, Nucl. Phys. **A126**, 361 (1969).
[50]S. Ohkubo, in Proceedings of the Fifth International Conference on Clustering Aspects in Nuclear and Subnuclear Systems, Kyoto, 1988, edited by Y. Sakuragi, T. Wada, and Y. Fujiwara (unpublished).
[51]H. Oeschler, H. Schröter, H. Fuchs, L. Baum, G. Gaul, H. Lüdecke, R. Santo, and R. Stock, Phys. Rev. Lett. **28**, 694 (1972).
[52]C. W. Towsley, D. Cline, and R. N. Horoshko, Nucl. Phys. **A204**, 574 (1973).
[53]P. Betz, E. Bitterwolf, B. Busshardt, and H. Röpke, Z. Phys. A **276**, 295 (1976).
[54]E. Bitterwolf, A. Burkard, P. Betz, F. Glatz, F. Heidinger, Th. Kern, R. Lehmann, S. Norbert, H. Röpke, C. Schneider, and J. Siefert, Z. Phys. A **313**, 123 (1983).
[55]L. Meyer-Schützmeister, A. J. Elwyn, S. A. Gronemeyer, G. Hardie, R. E. Holland, and K. E. Rehm, Phys. Rev. C **18**, 1148 (1978).
[56]I. P. Johnstone, Nucl. Phys. **A110**, 429 (1968).
[57]G. C. Ball, J. S. Forster, D. Ward, and C. F. Monahan, Phys. Lett. **37B**, 366 (1971).
[58]J. Styczen, J. Chevallier, B. Haas, N. Schulz, P. Taras, and M. Toulemonde, Nucl. Phys. **A262**, 317 (1976).
[59]P. Betz, H. Röpke, F. Glatz, G. Hammel, V. Glattes, and W. Brendler, Z. Phys. **271**, 195 (1974).
[60]Th. Kern, P. Betz, E. Bitterwolf, F. Glatz, and H. Röpke, Z. Phys. A **294**, 51 (1980).
[61]J. B. Mc Grory, B. H. Wildenthal, and E. C. Halbert, Phys. Rev. C **2**, 186 (1970).
[62]J. A. Becker, T. T. Bardin, T. R. Fisher, B. A. Watson, and E. K. Warburton, Phys. Rev. C **10**, 99 (1974).
[63]M. Toulemonde, J. Chevallier, B. Haas, N. Schulz, and J. Styczen, Nucl. Phys. **A262**, 307 (1976).
[64]H. J. Gils, H. Rebel, and E. Friedman, Phys. Rev. C **29**, 1295 (1984).
[65]D. Wintgen, H. Friedrich, and K. Langanke, Nucl. Phys. **A408**, 239 (1983).
[66]P. M. S. Lesser, D. Cline, P. Goode, and R. N. Horoshko, Nucl. Phys. **A190**, 597 (1972); G. D. Dracoulis, D. C. Radford, and A. R. Poletti, J. Phys. G **4**, 1323 (1978).